Dynamic and Steady-State Features of a Cooled Countercurrent Flow Reactor

Rohit Garg and Dan Luss
Dept. of Chemical Engineering, University of Houston, Houston, TX 77204

Johannes G. Khinast
Dept. of Chemical and Biochemical Engineering, Rutgers University, Piscataway, NJ 08854

A countercurrent flow reactor (CFR) is an autothermal reactor, in which the reactants flow countercurrently at equal velocities and flow rates through two compartments, with negligible heat-transfer resistance between the two sections. Two-reactor configurations can be used: a ''regular'' one, in which the two components are fed by two separate feeds; a ''folded'' configuration, in which a single feed flows first through one compartment and then reverses its direction and flows countercurrently in the second. Temperature and concentration profiles in the regular CFR configuration usually have mirror symmetry around its center. Under cooling, however, asymmetric steady-state profiles may form. The interaction between the heat removed by the effluents and by cooling through the wall may generate complex periodic or even chaotic states. The temperature and concentration profiles in a folded CFR are the same as those attained in a regular CFR, which are symmetric around the reactor center. The imposed symmetry causes the steady-state and dynamic features of the folded CFR to be less complicated than those of the regular CFR and is less likely to cause operational problems. Boundaries of parameter regions with qualitatively different features for both CFR configurations were constructed by the method of Khinast et al. (1998a). The analysis of the CFR enhances the understanding of similar dynamics observed in a reverse-flow reactor.

Introduction

Autothermal operation of chemical reactors, in which exothermic reactions are carried out, has attracted considerable interest over the past few years. It enables an energy-efficient operation, since the hot effluent heats up the feed to the reactor and no additional heat sources are required. A multifunctional reactor in which heat exchange and reaction occur simultaneously, in general, enables a more efficient autothermal operation than a combination of a chemical reactor and external heat exchanger. Significant recent activity involved the autothermal reverse-flow reactor (RFR) and the catalytic countercurrent flow reactor (CFR). In the RFR, a hot reaction zone is trapped in a packed bed by periodically reversing the flow direction. Adiabatic operation leads to periodic, *period-1* symmetric states at which the temperature (and concentration) profiles at the beginning and end of a flow-reversal period are mirror images. Previous studies by Rehacek et al. (1992, 1998), Salinger and Eigenberger (1996a,b), and Khinast et al. (1998a, 1999) show that cooling may generate more intricate dynamics in an RFR, such as asymmetric, quasi-periodic, or chaotic states. These complex dynamics usually are encountered for short flow-reversal periods. Matros (1996) and Matros and Bunimovich (1996) presented comprehensive reviews of RFR applications.

A CFR consists of two parallel compartments, filled with catalytic pellets, through which the reactants flow countercurrently at equal velocities and flow rates. The temperature in both compartments is essentially the same due to the high rate of heat-transfer between the two compartments and between the gas and catalyst. The CFR has certain operational advantages over those of an RFR. It is easier to operate and

Correspondence concerning this article should be addressed to D. Luss.

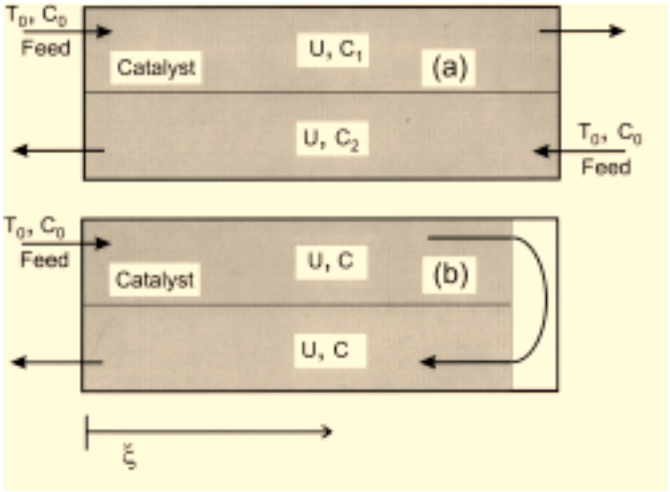

Figure 1. Two design possibilities of a cooled countercurrent flow reactor.

control, as it obviates the need for flow switching. It avoids the need to use and periodically replace high-quality valves, and circumvents the emission of not fully converted reactants during flow reversals, the so-called ''puff-volume'' (Gaiser, 1993; Sun et al., 1996; Friedrich et al., 1997).

The CFR can be designed in two different configurations: a ''regular'' one, in which the two compartments are fed by two separate feeds (Figure 1a), and a ''folded'' configuration (Figure 1b), in which the feed flows through one compartment and then in the reverse direction through the second compartment. In the regular CFR configuration (which for brevity will be referred to as CFR) the reactor temperature and the average cross-section concentration profiles usually have mirror symmetry around its center. Previous studies of the RFR dynamics suggest that cooling and heat losses in a CFR may generate asymmetric steady states and complex dynamics, like symmetric or asymmetric periodic states, or chaos. One goal of this study is to determine if and when these complex states are generated and to gain insight into the cause of their formation. As will be shown later, the maximum temperature of these complex states exceeds that of the symmetric steady-state solutions. This may damage the catalyst, initiate undesired reactions, or even lead to runaway. *A priori* knowledge of the onset of these undesired features is needed to avoid pitfalls in the CFR operation and control and to provide insight and knowledge into its operation. The analysis of the CFR enhances our understanding of similar dynamics of the reverse-flow reactor.

As we explain later, the two CFR configurations may not be equivalent and may attain different stable steady states and/or periodic states. One of our goals is to determine and explain the cause for this rather surprising difference.

Mathematical Model for Cooled CFR

We consider a CFR (Figure 1a), operating with equal feed flow rates and velocities in both directions. The same irreversible, exothermic, first-order reaction occurs in both compartments. The external reactor walls are maintained at a constant temperature by a coolant. We describe this countercurrent reactor by a one-dimensional, pseudohomogeneous model (Vortmayer and Schäfer, 1974), which assumes that the same temperature exists in both streams at any axial position. The rate expression also accounts for external mass-transfer resistance between the fluid and the catalyst. Our model accounts for axial heat-conduction and mass dispersion, and assumes that all the physical properties are independent of the temperature and concentrations. It ignores the pressure variation along the catalytic bed. To describe the RFR, Eigenberger and Nieken (1988), Matros (1989), Haynes et al. (1995), Seiler and Emig (1997), Khinast and Luss (1997), and Khinast et al. (1998a) have used pseudohomogeneous models. Dommeti et al. (1999) showed that the pseudohomogeneous and two-phase models have the same qualitative features for a single exothermic first-order reaction and a particle Lewis number, $Le_p = (h/\rho c_p)_g k_c$, exceeding unity, if

$$\frac{k(T_0)}{k_c a_v} < \exp\left\{4Le_p - 2 - \frac{E_a}{RT_0}\frac{(-\Delta H)c_0}{(\rho c_p)_g T_0}\right\}. \quad (1)$$

Table 1. Parameters Used in the Simulations

a_v	2,628.8 m^2_{Surf}/m^3_{React}	$T_0 = T_c$	323 K
D	4×10^{-5} m^2/s	ΔT_{ad}	50 K
E/R	8,328.6 K	ϵ	0.69
h	0.13 kW/m$^2\cdot$K	λ_s	1.26 W/m$\cdot$K
k_c	0.115 m/s	$(\rho c_p)_g$	0.6244 kJ/m$^3\cdot$K
k_∞	1.815×10^7 s^{-1}	$(\rho c_p)_s$	1,381.61 kJ/m$^3\cdot$K
L	1.0 m		

The set of parameters (Table 1) used in our study satisfies the preceding criterion. If a pseudohomogeneous model is assumed to be valid in the two compartments of the CFR, and the temperature in both compartments is the same at any axial position, then the energy balance of the CFR is

$$Le\frac{\partial\theta}{\partial\tau} - \frac{1}{\phi_h^2}\frac{\partial^2\theta}{\partial\xi^2} - \beta\cdot B(\theta)\cdot 0.5\cdot\left[(1-x_1)+(1-x_2)\right] + \Delta\cdot(\theta-\theta_c) = 0. \quad (2)$$

At each side of the CFR, feed enters one compartment and a hot effluent exits from the other compartment. Thus, the boundary conditions at either end are the average of the Danckwerts boundary conditions at one inlet and one outlet ($\partial\theta/\partial\xi = 0$), that is,

$$\frac{Da}{\phi_h^2}\frac{\partial\theta}{\partial\xi} = \frac{1}{2}(\theta-1) \qquad \text{at} \quad \xi = 0 \quad (3)$$

$$\frac{Da}{\phi_h^2}\frac{\partial\theta}{\partial\xi} = -\frac{1}{2}(\theta-1) \qquad \text{at} \quad \xi = 1. \quad (4)$$

The mass balance in each compartment is

$$\epsilon\frac{\partial x_1}{\partial\tau} - \frac{1}{\phi_m^2}\frac{\partial^2 x_1}{\partial\xi^2} + \frac{1}{Da}\frac{\partial x_1}{\partial\xi} - B(\theta)\cdot(1-x_1) = 0 \quad (5)$$

$$\epsilon\frac{\partial x_2}{\partial\tau} - \frac{1}{\phi_m^2}\frac{\partial^2 x_2}{\partial\xi^2} - \frac{1}{Da}\frac{\partial x_2}{\partial\xi} - B(\theta)\cdot(1-x_2) = 0, \quad (6)$$

with the corresponding boundary conditions:

$$\frac{Da}{\phi_m^2}\frac{\partial x_1}{\partial \xi} = x_1 \qquad \frac{\partial x_2}{\partial \xi} = 0 \qquad \text{at} \quad \xi = 0 \tag{7}$$

$$\frac{Da}{\phi_m^2}\frac{\partial x_2}{\partial \xi} = -x_2, \qquad \frac{\partial x_1}{\partial \xi} = 0 \qquad \text{at} \quad \xi = 1, \tag{8}$$

where subscript 1 (2) indicates flow from the left (right).

The dimensionless state variables in the preceding equations are

$$\theta = \frac{T}{T_0}, \qquad x = \frac{c_0 - c}{c_0}, \qquad \tau = t \cdot k(T_0), \qquad \xi = \frac{z}{L}. \tag{9}$$

The dimensionless groups are:

$$\Psi = \frac{(\rho c_p)_s}{(\rho c_p)_g}, \qquad Le = \Psi \cdot (1-\epsilon) + \epsilon, \qquad \theta_c = \frac{T_c}{T_0},$$

$$\phi_h^2 = \frac{L^2 \cdot k(T_0) \cdot (\rho c_p)_g}{\lambda_{ax}}, \quad \phi_m^2 = \frac{L^2 \cdot k(T_0)}{\epsilon \cdot D_{ax}}, \quad \gamma = \frac{E_a}{R \cdot T_0},$$

$$Da = \frac{L \cdot k(T_0)}{u}, \qquad \Delta = \frac{2 \cdot U}{r \cdot (\rho c_p)_g \cdot k(T_0)}, \qquad \beta = \frac{\Delta T_{ad}}{T_0},$$

$$B(\theta) = \frac{a_v \cdot k_c \cdot \exp\left[\gamma\left(\frac{\theta - 1}{\theta}\right)\right]}{a_v \cdot k_c + k(T)} = \frac{\frac{a_v \cdot k_c}{k(T_0)}}{1 + \frac{a_v \cdot k_c}{k(T)}}, \tag{10}$$

where

$$k(T) = k_\infty \cdot \exp\left[-\frac{\gamma}{\theta}\right]. \tag{11}$$

The temperature and concentration profiles of the folded CFR are obtained by solving only Eqs. 2 and 5 and requiring symmetry of the temperature (but not of the conversion), that is, $\Theta(\xi) = \Theta(1-\xi) \forall \xi < 0.5$. The steady-state equations are obtained by deleting the time derivatives from the preceding set of partial differential equations. The transient behavior was computed by a finite-differences scheme (discretizing the spatial variables by 100 node points) and integrating Eqs. 2, 5, and 6 with LIMEX (Deuflhard et al., 1987), an extrapolation-solver designed for large differential–algebraic systems.

Dynamic Features of Model

Numerical simulations were carried out to determine the behavioral features of a CFR with the flow configuration shown in Figure 1a. The base-case parameters used in the simulations are reported in Table 1. The values of the dimensionless groups for a superficial gas velocity of 1.5 m/s are:

$$\Psi = 2213 \qquad Le = 687 \qquad \phi_h^2 = 2.43 \times 10^{-2}, \qquad \phi_m^2 = 4.16,$$

$$\gamma = 25.8 \qquad Da = 7.66 \times 10^{-5}, \qquad \beta = 0.155. \tag{12}$$

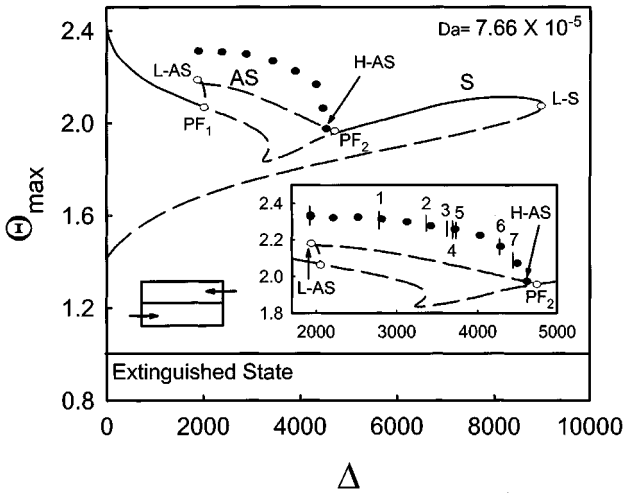

Figure 2. Bifurcation diagram of the maximum CFR temperature, θ_{max} vs. the cooling capacity, Δ.

Insert describes bifurcation points discussed in text. S (AS) = symmetric (asymmetric) steady-states; PF = pitchfork bifurcation; H-S (-AS) = Hopf bifurcation on symmetric (asymmetric) steady-state branch; L-S (-AS) = limit point of symmetric (asymmetric) steady-states; solid circle = periodic or chaotic state; open circle = singular point; solid line = stable; dashed line = unstable.

The Damköhler number, *Da*, which is the ratio between the residence time in the reactor to the characteristic reaction time, is inversely proportional to the reactant velocity.

A typical bifurcation diagram of the maximum CFR temperature vs. the cooling capacity (Δ) is shown in Figure 2. An ignited state exists for all cooling capacities smaller than that of the limit point of the branch of the symmetric steady states (denoted as L-S in Figure 2). Most steady states of the CFR are *symmetric*, that is, the temperature and concentration profiles have mirror symmetry about the center of the reactor. However, some asymmetric steady-state solutions exist. Note that a mirror image of any asymmetric steady state is also a steady state of the CFR. The temperature profiles of an unstable symmetric and a stable asymmetric steady state for $\Delta = 4{,}700$ are shown in Figure 3. The branch of symmetric steady states, shown in Figure 2, becomes unstable at either one of the two pitchfork (PF) bifurcations. At the pitchfork point PF_2 ($\Delta = 4{,}805$), a supercritical branch of stable *asymmetric steady states* emanates, while at PF_1 ($\Delta = 2{,}060$) a subcritical branch of unstable asymmetric steady states emanates. Stability analysis shows that most asymmetric steady-state solutions are unstable. The asymmetric steady state becomes unstable at a supercritical Hopf bifurcation, H-AS, at $\Delta = 4{,}644$, at which a branch of periodic solutions emerges (shown as dots in Figure 2). As is shown below stable periodic or aperiodic states exist between points L-AS and H-AS of the unstable branch of asymmetric states in the inset in Figure 2.

Similar to the RFR (Khinast et al., 1998a), the CFR temperature profiles have a flat plateau in the center of the reactor under adiabatic operation (Figure 4). With no wall cooling, all the heat is lost via convection by the effluents. Under low cooling, the steady-state temperature profiles have two

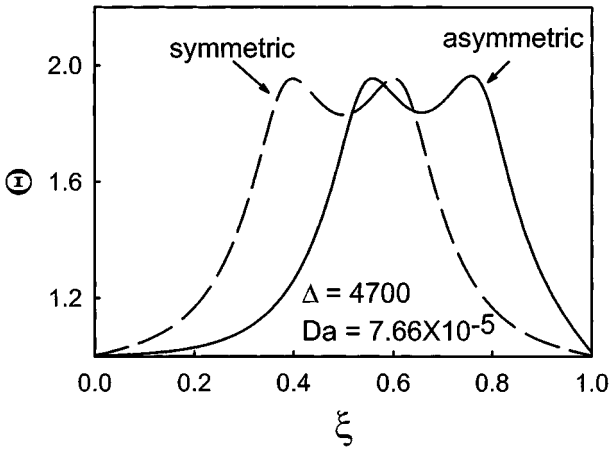

Figure 3. Dimensionless temperature profiles of the unstable symmetric and stable asymmetric steady states of the CFR.

maxima ($\Delta = 1{,}500$ in Figure 4) as the cooling quenches the reaction in the middle of the reactor. Increasing the cooling capacity decreases the ratio between the convective heat loss to that removed through the wall, and shifts the two maxima to the reactor center ($\Delta = 5{,}000$). Eventually at a very high rate of external cooling the two peaks coalesce into one ($\Delta = 8{,}000$) and essentially all the heat is removed through the walls. Further increase of the cooling eventually leads to extinction.

We define a periodic state to have *spatiotemporal* symmetry if any profile is transformed to its mirror image after half a period later. This behavior is also referred to as *discrete rotating wave symmetry* in the mathematical literature.

The simplest and most common nonstationary state is of period 1. Figure 5 describes six snapshots of the temperature (solid line) and reactant concentrations (dashed lines) profiles in the two compartments for half a period of a symmetric period-1 oscillation. During this half-period, the temperature peak next to the right side of the reactor ($\tau/P = 0$ to 0.3

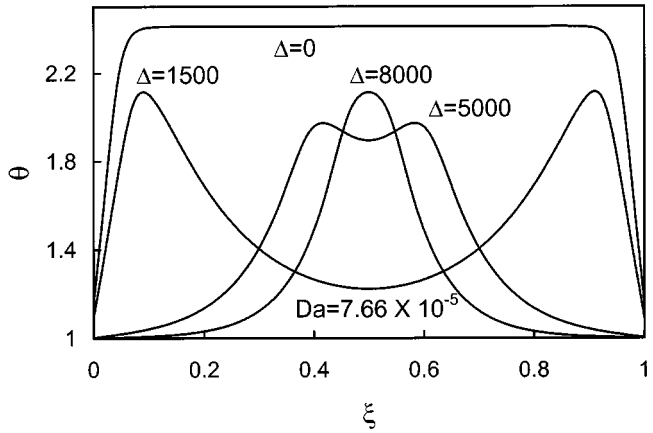

Figure 4. Influence of the cooling capacity, Δ, on the dimensionless temperature (θ) profiles for symmetric steady states.

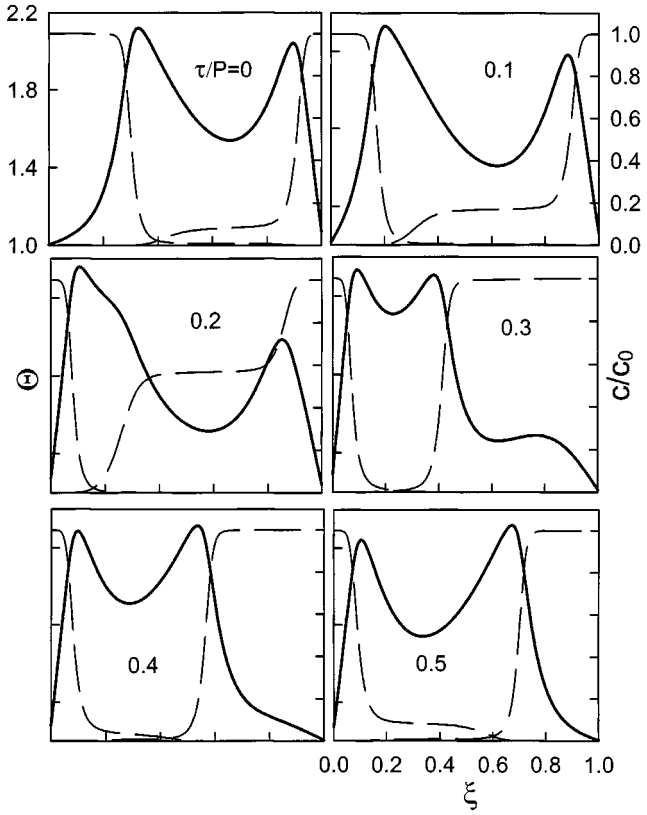

Figure 5. Temperature and concentrations profiles in the CFR at various times during half a period of a symmetric period-1 state, with period, *P*, of 1.8 at $\Delta = 2{,}400$ and $Da = 7.66 \times 10^{-5}$.

Solid (dashed) line denotes dimensionless temperature (concentration) profile.

in Figure 5) extinguishes due to wall-cooling. Consequently, the feed entering from the right is only partly converted at

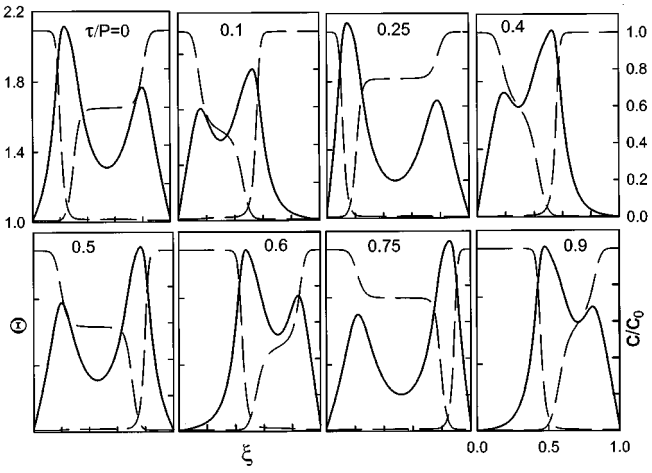

Figure 6. Temperature and concentrations profiles in the CFR at various times during one period of a symmetric period-2 state, with period, *P*, of 5.21 at $\Delta = 3600$ and $Da = 7.66 \times 10^{-5}$.

Solid (dashed) line denotes dimensionless temperature (concentration) profile.

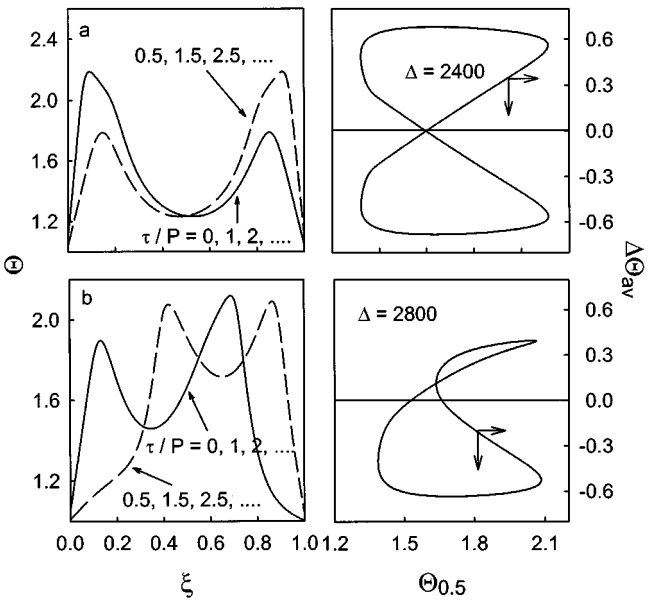

Figure 7. Dimensionless temperature profiles and corresponding phase plane for: a) symmetric period-1 state, with period, *P*, of 1.8; b) asymmetric period-1 state with $P = 1.2$. $Da = 7.66 \times 10^{-5}$ in both cases.

this low-temperature peak, and its conversion is completed at the higher temperature peak on the left. This causes the left temperature peak to become higher and move to the right. Subsequently, cooling splits the temperature peak on the left into two ($\tau/P = 0.3$) and causes their separation. The process is reversed as the high-temperature maximum approaches the left reactor end ($\tau/P = 0.3$–0.4) and much heat is withdrawn by convection of the effluent at the left exit. This decreases the maximum temperature and respective conversion and increases the temperature of the right-moving peak ($\tau/P = 0.4$–0.5). Thus, after half a period ($\tau/P = 0.5$) the temperature profile is a mirror image of the initial one ($\tau/P = 0$). The second half of this symmetric motion is a mirror image of that in the first and is associated with the extinction of the temperature peak on the other (left) side of the reactor. If we denote by R (L) an increase of the reactant concentration on the right (left) side of the reactor, these period-1 motions can be described by the repeated sequence of LRLRLR . . . motion.

Period n motions involve an intricate sequence of $2n$ concentration buildups. For example, a symmetric period-5 state (shown later in Figure 10) consists of the sequence RRLLRLLRRL. The symmetric period-2 motion in Figure 6 consists of the sequence RRLL, that is, two successive reactant concentration buildups on the righthand side of the reactor for τ/P between (0 and 0.1) and (0.25 and 0.40), followed by two successive reactant concentration buildups on the lefthand side for τ/P between (0.5 and 0.6) and (0.75 and 0.9). In some cases, the reactant concentration increase and thermal con-

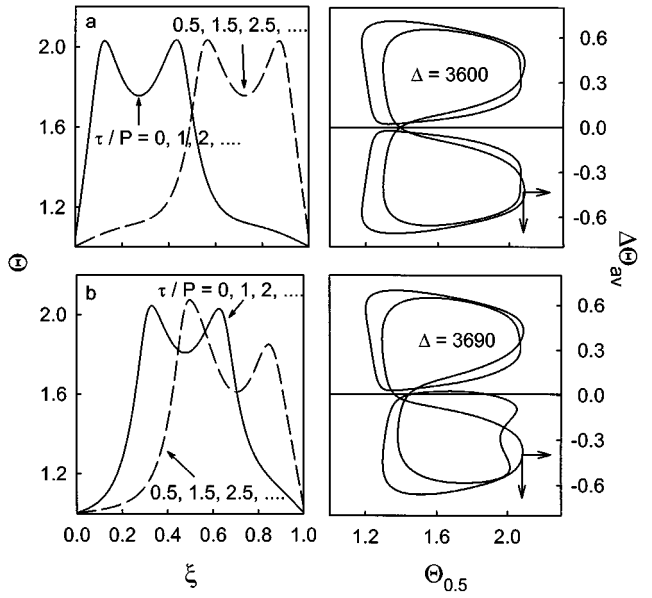

Figure 8. Dimensionless temperature profiles and corresponding phase plane for: a) symmetric period-2 state with period, *P*, of 5.21; b) asymmetric period-2 state with $P = 4.79$.

$Da = 7.66 \times 10^{-5}$ in both cases.

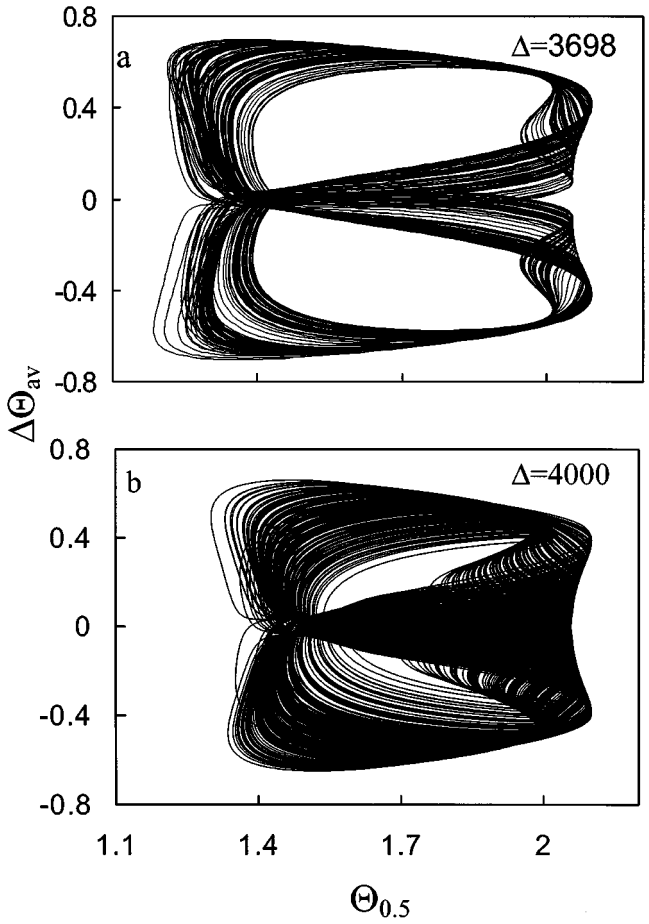

Figure 9. Phase plane of chaotic motion at $Da = 7.66 \times 10^{-5}$.

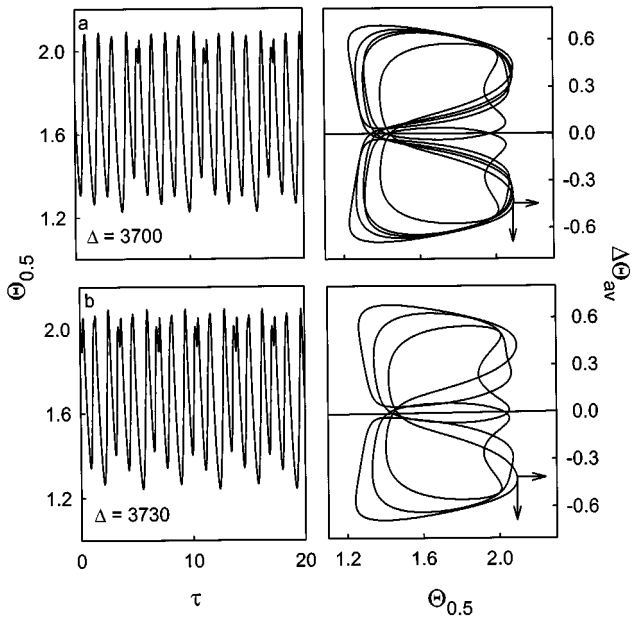

Figure 10. Dimensionless time series of CFR center temperature, $\theta_{0.5}$, and corresponding phase plane at $Da = 7.66 \times 10^{-5}$.

duction from an adjacent temperature peak cause a temperature peak moving towards a reactor end to reverse the direction of its motion.

Phase planes of periodic and aperiodic states of the CFR, for Δ values between the L-AS and H-AS points in the inset of Figure 2, are depicted in Figures 7 to 10. Each phase plane describes the dependence of the reactor center temperature, $\theta_{0.5}$, on the difference between the average temperature of the left and right half of the CFR, $\Delta\theta_{av}$. The phase plane of a spatiotemporal symmetric (asymmetric) periodic state is symmetric (asymmetric) around the abscissa. A periodic motion of *period* "*n*" consists of *n* loops in the phase plane. Note that Figures 7 and 8 show profiles at a particular time and at half a period later, but do not bound the temperature oscillations.

Spatiotemporal symmetric period-1 states, for which each temperature profile is a mirror image of that half a period later (Figure 7a), exist between points L-AS ($\Delta = 1{,}874$) and 1 ($\Delta = 2{,}765$) in the inset in Figure 2, between points 2 ($\Delta = 3{,}335$) and 3 ($\Delta = 3{,}590$), and between points 7 ($\Delta = 4{,}410$) and H-AS. In all these cases, the time-averaged temperature distribution in the CFR is symmetric around its center. Asymmetric period-1 states exist between points 1 and 2, and between points 6 ($\Delta = 4{,}250$) and 7. These asymmetric period-1 states (Figure 7b) are periodic, but any profile is not a mirror image of that at the preceding half-period. Note that any mirror image of an asymmetric periodic state is also a periodic state of the CFR and the phase portrait of one is a mirror image of the other. Spatiotemporal symmetric period-2 states exist between points 3 and 4 ($\Delta = 3{,}675$), while asymmetric period-2 states appear between points 4 and 5 ($\Delta = 3{,}692$). Corresponding temperature profiles and phase-plane portraits are shown in Figure 8. The doubling of the period is apparent from the doubling in the number of loops in the phase portrait.

A chaotic state forms when both the symmetric and asymmetric periodic states become unstable and interfere with each other. Chaotic states exist between points 5 and 6 in the inset in Figure 2. The transition to the chaos occurs via an intermittency scenario. Figure 9 shows the phase plane of two chaotic states. Narrow windows of period-*n* states (spatiotemporal symmetric or asymmetric) were interdispersed in this chaotic region. For example, Figure 10 shows a symmetric period-5 and an asymmetric period-3 state existing within this region. Numerical simulations show that chaotic states exist only for a limited range of intermediate *Da* values. For example, all the solutions on the branch between L-AS and H-AS in Figure 2 are periodic for $Da = 5.47 \times 10^{-5}$. This value may be attained by increasing the reactant velocity of the case shown in Figure 2 by 40%.

Experience with an exothermic reaction carried out in a continuous-stirred tank reactor teaches that complex behavior usually occurs due to a competition between the rate of cooling through the wall and the convective heat removal by the effluent. A similar situation occurs in the CFR. At low *Da* (or equivalently large superficial velocity) the reactor effluents remove most of the reaction heat generated in the CFR. At very large *Da* (or equivalently small superficial velocity) most of the reaction is completed in a very narrow region next to the reactor inlets. Again in this case, most of the reaction heat is removed by the reactor effluents and not through the reactor walls. A different situation arises for intermediate Damköhler numbers. As Figure 4 shows, the reaction may be either quenched in the reactor center so that some heat is convected out of the reactor by the effluents or that the reaction occurs only in the center of the reactor and all the reaction heat is removed through the wall. The transition between the two cases generates periodic instabilities and the simultaneous movement of the quenched regions. These heuristic arguments explain why a CFR does not exhibit asymmetric steady-states or complex dynamics at either very high or low *Da* values.

The maximum temperature of any asymmetric steady state exceeds that of the corresponding unstable symmetric steady state. The maximum temperature of the periodic or chaotic states is even higher. Thus, asymmetric steady states and periodic or aperiodic states may lead to excessively high temperatures, which can damage the catalyst and initiate undesired reactions that do not occur at lower temperatures. To avoid these undesired states, it is essential to know when they occur.

Construction of Bifurcation Maps

Following the method described by Golubitsky and Schaeffer (1985), Balakotaiah and Khinast (1998), Khinast et al. (1998b) and Luss and Khinast (1999), we construct bifurcation maps of parameter regions with qualitatively different steady states and dynamic features to obtain a better insight and understanding of the robustness of these features. The loci of the pitchfork and limit-point singularities satisfy the conditions:

$$F(u_0, \lambda_0) = 0 \tag{13}$$

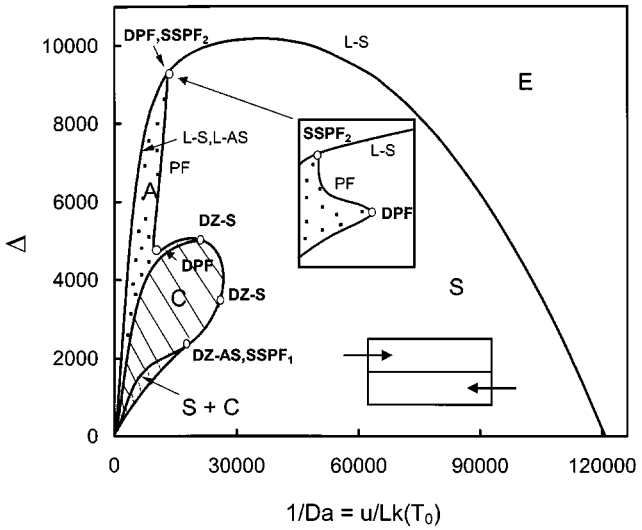

Figure 11. Map of regions with qualitatively different behavior.

S, A, and E denote regions in which CFR exhibits symmetric, asymmetric, and extinguished steady-states, respectively, and C denotes complex dynamic behavior. PF = pitch-fork; L-S (-AS) = limit point of the symmetric (asymmetric) steady-state solutions; H-S (-AS) = Hopf bifurcation on symmetric (asymmetric) steady-state branch; DZ-AS = double-zero point on asymmetric steady-state branch; SSPF = sub-supercritical pitchfork bifurcation; DZ-S = double-zero point on symmetric steady-state branch; DH = degenerate Hopf bifurcation; DPF = degenerate pitchfork.

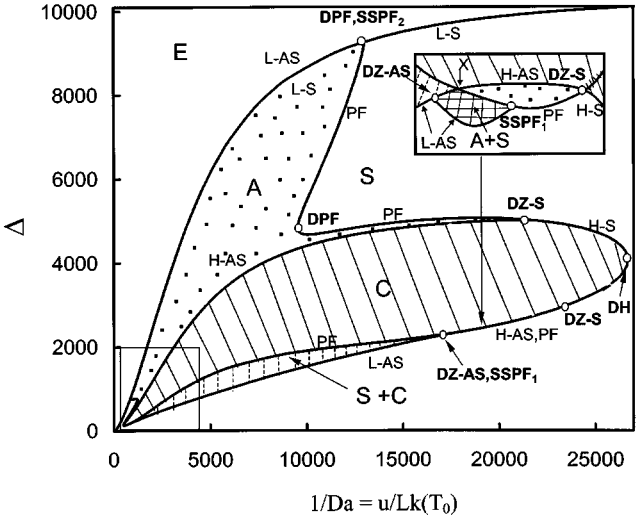

Figure 12. Enlarged portion of Figure 11.

The insert is the region close to DZ-AS, $SSPF_1$, and DZ-S. Both symmetric and asymmetric steady states coexist in the crosshatched region in the insert.

$$\left[D_u F(u_0,\lambda_0)\right]\cdot Y = 0 \tag{14}$$

$$Y\cdot Y = 1, \tag{15}$$

where F is the set of model equations, u is a state vector, λ is the bifurcation parameter, and u_0 the solution for $\lambda = \lambda_0$. $D_u F(u_0,\lambda_0)$ is the Jacobian matrix evaluated at (u_0,λ_0), and Y is its eigenvector for a zero eigenvalue. The normalization condition (Eq. 15) is introduced to avoid getting a trivial solution.

A branch of periodic solutions emerges at a Hopf bifurcation that satisfies the following conditions:

$$F(u_0,\lambda_0) = 0 \tag{16}$$

$$\left[D_u F(u_0,\lambda_0)\right]\cdot Y = \mu_i Y \tag{17}$$

$$Y\cdot Y = 1 + i, \tag{18}$$

where μ_i is the absolute value of the purely imaginary eigenvalue of $D_u F(u_0,\lambda_0)$. Equation 18 is a normalization condition.

To calculate the bifurcations loci, we discretize the spatial variables by a finite differences scheme with 100 node points and solve the resulting equations using Broyden's method (Broyden, 1965). A pseudo-arc-length continuation technique (Keller, 1977) was used to construct branches of the steady states and the singular points. Figure 11 is a bifurcation map in the plane of the cooling capacity vs. the Damköhler number showing the loci of these three singular points (limit, pitchfork, and Hopf). We vary the Damköhler number by changing the superficial velocity only. Some bifurcation loci are so close to each other that they cannot be distinguished in Figure 11. Thus, we present more detailed maps of some regions (Figures 12 and 13), which show the fine structure of some of the transitions. In the Appendix we present a brief description of the transitions that occur at the codimension-2 singular points, at which two bifurcation loci of codimension-1 (limit, pitchfork, and Hopf) coalesce. Examples of such points in Figure 11 are the double-zero point on the asymmetric branch (DZ-AS), double-zero point on the symmetric branch (DZ-S), and sub-supercritical pitchfork bifurcation (SSPF).

The bifurcation map, Figure 11, shows that a high-temperature state exists in addition to the extinguished state within

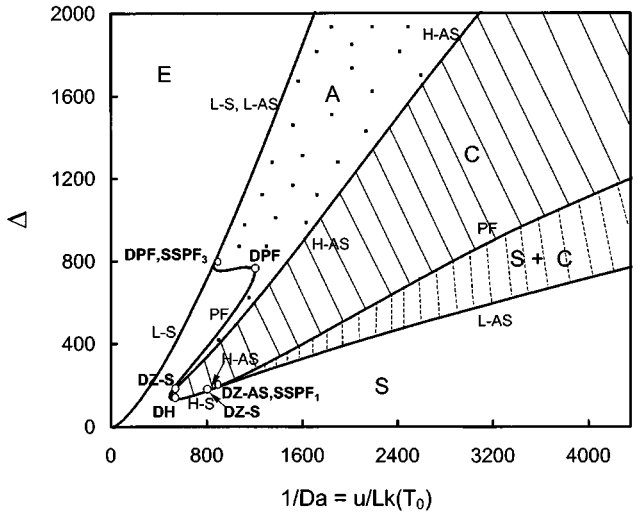

Figure 13. Englargement of the rectangular area in Figure 12.

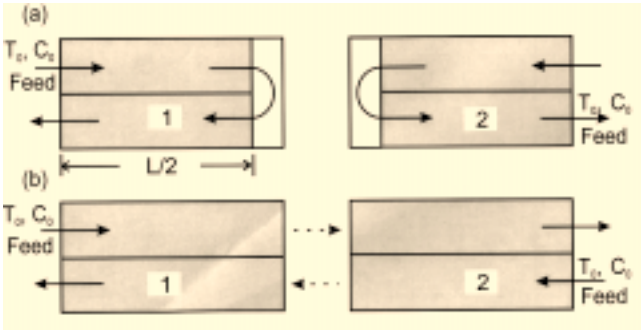

Figure 14. (a) Two "folded" configuration CFRs placed back to back; (b) the same configuration with the CFR on the right turned upside down so that the flow in the two bottom compartments is countercurrent to those on top.

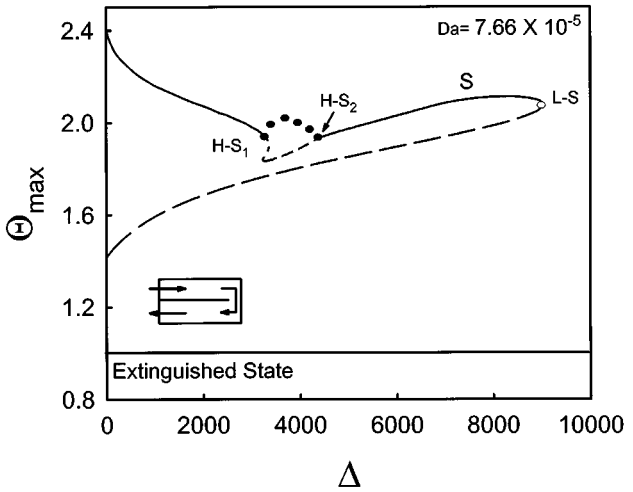

Figure 15. Bifurcation diagram of the maximum folded CFR temperature, θ_{max} vs. the cooling capacity, Δ.

S = symmetric steady-states; H-S = Hopf bifurcation on symmetric steady-state branch; L-S = limit point of symmetric steady states; solid circle = periodic state; open circle = singular point; solid line = stable; dashed line = unstable.

the bell-shaped region, bounded by the loci of the limit point of the symmetric steady states (L-S) and the limit points of the asymmetric steady states (L-AS). For *Da* numbers larger than the one corresponding to $SSPF_2$, the loci of L-S and L-AS are very close to each other and indistinguishable in Figure 11. Only extinguished states exist outside the bell-shaped region for small and large *Da* values (i.e., short and long residence times) and high cooling capacities. Symmetric steady states exist in most of the bell-shaped region and are the only ignited states that exist for small *Da* values, or under adiabatic operation ($\Delta = 0$). Complex dynamic behavior (denoted as hatched region C in Figures 11–13) occurs only at intermediate cooling capacities and large *Da* values, that is, high residence times. Asymmetric steady states (denoted as dotted region A) exist only at high cooling capacities and large *Da* values. Figures 12 and 13 indicate that the transitions between the various regions are rather intricate. In Figure 12, it can be seen that stable symmetric and stable periodic states coexist in a small region (S + C). Depending on the initial conditions one of these states is reached. Figure 13 shows the bifurcations behavior close to the origin of the plane. The existence of these very narrow regions and bifurcations is mainly of academic interest.

Performance of the Folded CFR

Figure 14a shows two "folded" CFRs placed back-to-back. Clearly, the temperature and concentration profiles in one are a mirror image of those in the second. Figure 14b shows the same configuration with the CFR on the right turned upside down, so that the flow in the two bottom compartments is countercurrent to the two on top. Enabling the flow in the bottom and top sections to proceed with no direction reversal at $L/2$ transforms these two folded CFRs to a "regular" CFR, the temperature profile of which is symmetric with respect to its center. We conclude that the temperature and concentration profiles in the "folded" CFR are identical to those in a regular CFR with symmetric states. In other words, a folded CFR behaves as a regular CFR on which we impose a symmetry condition. It is well known that imposing symmetry on a mathematical model may decrease the set of possible steady states, affect the stability of the steady states, and change the nature of the dynamic behavior. Below we describe the influence of this imposed symmetry on the behavior of the folded CFR. It is important to note that the symmetry in the temperature profile of the folded CFR is due to the assumption of negligible heat-transfer resistance between the two compartments. When this common assumption is not valid it will affect the behavioral features of the two CFR configurations. We proceed with the analysis of the case for which the temperature in the top and bottom compartments depends only on the distance from the point at which the flow reverses its direction (reactor center), that is, the temperature profile is symmetric around the reactor center.

Figure 15 is a bifurcation diagram of a folded CFR operating under the same conditions as those used to produce the bifurcation diagram of the regular CFR (Figure 2). A comparison of the two bifurcation diagrams indicates that both the folded and regular CFR have the same branch of symmetric steady states. However, the regular CFR may attain stable asymmetric steady states (see, for example, Figure 3), while the folded CFR cannot attain any asymmetric steady states. The periodic states of the folded CFR emanate from the branch of symmetric steady states. The periodic solutions of the regular CFR emanate from Hopf points on the branch of asymmetric states. While the folded CFR has periodic states for Δ values between 3311 and 4290, the regular CFR has periodic and aperiodic states for a much larger range of Δ values (1874 to 4644). Another important difference is that the temperature profiles of the periodic states of the folded CFR are symmetric about the center, while the regular CFR has some asymmetric periodic states.

Figure 16 is a bifurcation map of the folded CFR. Comparing it with Figure 11, constructed for the regular CFR, shows that in both cases the same locus of the limit point of the symmetric steady states bounds the region in which an ig-

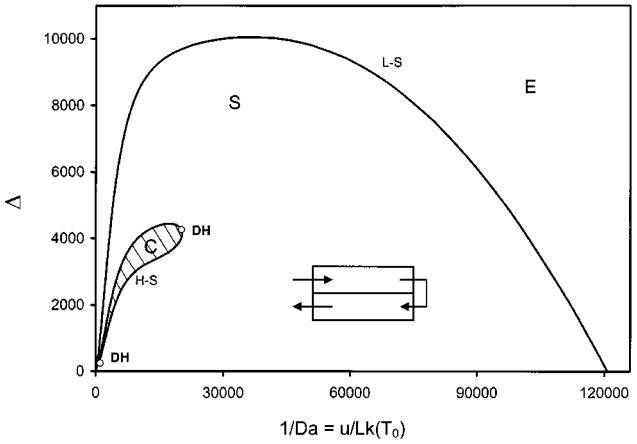

Figure 16. Map of regions with qualitatively different behavior of a folded CFR.

S and C denote regions exhibiting symmetric steady state and complex dynamics behavior, respectively. L-S = limit point of the symmetric solutions; H-S = Hopf bifurcation on symmetric branch; DH = degenerate Hopf bifurcation.

nited state exists. The region of parameters in which the folded CFR attains periodic states is much smaller than that of the regular CFR. Moreover, while the CFR attains asymmetric steady and periodic states, the folded CFR does not attain any of these states.

Discussion and Conclusions

The bifurcation maps provide useful insight into the operation and control of the CFR. The CFR has nonextinguished states only for cooling capacities that are not too high and for Damköhler (*Da*) values that are not too small. Our study indicates that the CFR has a robust symmetric steady state over a wide range of operating conditions. However, under sufficient cooling capacity and intermediate *Da* values, the interplay between the cooling through the wall and convection by the effluents may generate nonsymmetric steady states and complex dynamic behavior, including chaos. At very high or low *Da* numbers, most of the heat is lost by convection, and only symmetric steady states exist. The maximum temperature of asymmetric steady states and complex dynamic states is higher than that of the symmetric steady states. These states should be avoided to ensure reactor safety. The bifurcation maps in Figures 12 and 13 shows that a symmetric steady state may coexist with either an asymmetric steady state or a periodic state in some very small parameter regions. The insight gained about the dynamics of CFR is most helpful in enhancing our understanding of similar dynamic behavior of the RFR.

The analysis of the behavior of a folded CFR clearly points out the important impact of imposed symmetry on the nature and stability of its states. The imposed symmetry eliminates the possible existence of asymmetric steady states, increases the parameter regions in which stable ignited steady states exist, changes the nature of the periodic states, and decreases the size of the parameter region, in which complex dynamic behavior occurs. This suggests that the operation of folded-configuration CFR is more robust and less likely to lead to pitfalls due to dynamic instabilities than that of the regular CFR. Assuming that the behavior of the folded and regular CFR is equivalent may lead to surprising pitfalls. We are not aware of any reported study of the impact of imposed symmetry on the nature and stability of the performance of a chemical reactor.

The CFR and the RFR are two possible configurations of autothermal operation of packed-bed reactors. Other configurations include the rotating packed bed (Eigenberger and Nieken, 1991) and the circulation-loop reactor (Lauschke and Gilles, 1994). The internal heat-exchange in these autothermal reactors has some definite advantages over the use of external heat-exchangers. It is important to enhance our understanding of the behavioral features of these autothermal reactors to select the proper one for specific applications, to avoid pitfalls in their design and operation, and to provide a rational basis for the design of a proper control policy.

Acknowledgments

We gratefully acknowledge the financial support by the ACS-PRF and the Mobil Foundation. We are thankful to Prof. G. Eigenberger for insightful, helpful comments.

Notation

a_v = specific surface area, m^2_{Surf}/m^3_{React}
$B(\theta)$ = temperature dependence of reaction rate
c = concentration, mol/m^3
c_p = heat capacity, $J/(mol \cdot K)$
Da = Damköhler number
D_{ax} = axial diffusion constant, m^2/s
$D_u F$ = Jacobian matrix of F
E_a = activation energy, J/mol
F = set of model equations
h = heat-transfer coefficient between fluid and catalyst, $W/(K \cdot m^2)$
$-\Delta H$ = heat of reaction, J/mol
k_c = mass-transfer coefficient, m/s
k_∞ = frequency factor, 1/s
$k(T)$ = rate constant at temperature T, 1/s
L = reactor length, m
Le = Lewis number
Le_p = particle Lewis number
P = time period
r = outer reactor radius, m
R = universal gas constant, $J/(mol \cdot K)$
t = time, s
T = temperature, K
T_c = cooling temperature, K
T_{exit} = reactor effluent temperature, K
ΔT_{ad} = adiabatic temperature rise, $-\Delta H c_0/(\rho C_p)_g$, K
u = superficial gas velocity, m/s
$\mathbf{u}$ = state vector
U = overall heat-transfer coefficient, $W/(K \cdot m^2)$
x = conversion
Y = eigenvector of $D_u F$
z = axial coordinate, m

Greek letters

β = dimensionless adiabatic temperature rise
Δ = cooling capacity
ϵ = bed voidage
γ = dimensionless activation energy
λ = bifurcation parameter
λ_{ax} = effective axial thermal conductivity, $W/(m \cdot K)$
μ = eigenvalue of $D_u F$
ξ = dimensionless axial position
ρ = density, kg/m^3

τ = dimensionless time
θ = dimensionless temperature
θ_c = dimensionless cooling temperature
ϕ_h^2 = heat-transport modulus
ϕ_m^2 = mass-transfer modulus
Ψ = gas-to-solid volumetric heat-capacity ratio

Indices

1(2) = compartment in which flow is from the left (right)
g = gas phase
s = solid phase
0 = feed

Literature Cited

Balakotaiah, V., and J. Khinast, "Numerical Bifurcation Techniques for Chemical Reactor Problems," *IMA Proc. Num. Meth. for Bifurcation Problems*, Springer Verlag, New York (1998).

Broyden, C. G., "A Class of Methods for Solving Nonlinear Simultaneous Equations," *Math. Comput.*, **19**, 577 (1965).

Deuflhard, P., E. Hairer, and J. Zugck, "One-Step and Extrapolation Methods for Differential—Algebraic Systems," *Numer. Math.*, **51**, 1 (1987).

Dommeti, M. S. S., V. Balakotaiah, and D. H. West, "Analytical Criteria for Validity of Pseudohomogeneous Models of Packed-Bed Catalytic Reactors," *Ind. Eng. Chem. Res.*, **38**, 767 (1999).

Eigenberger, G., and U. Nieken, "Catalytic Combustion with Periodic Flow Reversal," *Chem. Eng. Sci.*, **43**, 2109 (1988).

Eigenberger, G., and U. Nieken, "Katalytische Abluftreinigung: Verfahrenstechnische Aufgaben und neue Lösungen," *Chem. Ing. Tech.*, **63**, 781 (1991).

Friedrich, G., G. Gaiser, G. Eigenberger, G. Opferkuch, and G. Kolios, "Kompakter Reaktor für katalytische Reactionen mit integriertem Wärmerücktausch," German Patent Application, DE 197 25 378 A1 (priority 16/6/1997).

Gaiser, G., "Reaktor zur katalytischen Behandlung gasförmiger Fluide," European Patent EP 0638140 B1 (priority 24/4/1993).

Golubitsky, M., and Schaeffer, D. G., *Singularities and Groups in Bifurcation Theory*, Vol. 1, Springer-Verlag, New York (1985).

Haynes, T. N., C. Georgakis, and H. S. Caram, "The Design of Reverse Flow Reactors for Catalytic Combustion Systems," *Chem. Eng. Sci.*, **50**, 401 (1995).

Keller, H. B., *Application of Bifurcation Theory*, Academic Press, New York (1977).

Khinast, J., A. Gurumoorthy, and D. Luss, "Complex Dynamic Features of a Cooled Reverse-Flow Reactor," *AIChE J.*, **44**, 1128 (1998a).

Khinast, J., D. Luss, M. P. Harold, J. J. Ostermaier, and R. McGill, "Continuously Stirred Decanting Reactor: Operability and Stability Considerations," *AIChE J.*, **44**, 372 (1998b).

Khinast, J., and D. Luss, "Mapping Regions with Different Bifurcation Diagrams of a Reverse Flow Reactor," *AIChE J.*, **43**, 2034 (1997).

Khinast, J., Y. O. Jeong, and D. Luss, "Dependence of Cooled Reverse-Flow Reactor Dynamics on Reactor Model," *AIChE J.*, **45**, 299 (1999).

Luss, D., and J. Khinast, *Scientific Computing in Chemical Engineering*, Springer-Verlag, Hamburg, 12 (1999).

Lauschke, G., and E. D. Gilles, "Circulating Reaction Zones in a Packed-Bed Loop Reactor," *Chem. Eng. Sci.*, **49**, 5359 (1994).

Matros, Yu. Sh., *Catalystic Processes under Unsteady-State Conditions*, Elsevier, Amsterdam (1989).

Matros, Yu. Sh., "Forced Unsteady-State Processes in Heterogeneous Catalytic Reactors," *Can. J. Chem. Eng.*, **74**, 566 (1996).

Matros, Yu. Sh., and G. A. Bunimovich, "Reverse-Flow Operation in Fixed Bed Catalytic Reactors," *Cat. Rev. Sci. Eng.*, **38**, 1 (1996).

Rehacek, J., M. Kubicek, and M. Marek, "Modeling of a Tubular Reactor with Flow Reversal," *Chem. Eng. Sci.*, **47**, 2897 (1992).

Rehacek, J., M. Kubicek, and M. Marek, "Periodic, Quasiperiodic and Chaotic Spatiotemporal Patterns in a Tubular Catalytic Reactor with Periodic Flow Reversal," *Comput. Chem. Eng.*, **22**, 283 (1998).

Salinger, A. G., and G. Eigenberger, "The Direct Calculation of Periodic States of the Reverse-Flow Reactor: 1. Methodology and Propane Combustion Results," *Chem. Eng. Sci.*, **51**, 4903 (1996a).

Salinger, A. G., and G. Eigenberger, "The Direct Calculation of Periodic States of the Reverse-Flow Reactor: 2. Multiplicity and Instability," *Chem. Eng. Sci.*, **51**, 4915 (1996b).

Seiler, H., and G. Emig, "Reduction-Oxidation-Cycling in a Fixed Bed Reactor with Periodic Flow Reversal," *Proc. Int. Symp. on Dynamics and Reaction Kinetics in Heterogeneous Catalysis*, Antwerpen, Belgium (1997).

Sun, Q., B. Young, D. F. Williams, D. Glasser and D. Hildebrandt, "A Periodic Flow Reversal Reactor: An Infinitely Fast Switching Model and a Practical Proposal for Its Implementation," *Can. J. Chem. Eng.*, **74**, 760 (1996).

Vortmeyer, D., and R. J. Schaefer, "Equivalence of One- and Two-Phase Models for Heat Transfer Processes in Packed Beds: One Dimensional Theory," *Chem. Eng. Sci.*, **28**, 484 (1974).

Appendix

The codimension of a singular point is the number of parameters that have to be varied (perturbed) in order to generate all the possible features (unfoldings) next to that point. A transversal or tangential intersection of two codimension-1 singularities is a codimension-2 singular point. Using the set of base parameters listed in Table 1, we found six different codimension-2 singularities, whose unfoldings are shown in Figure A1.

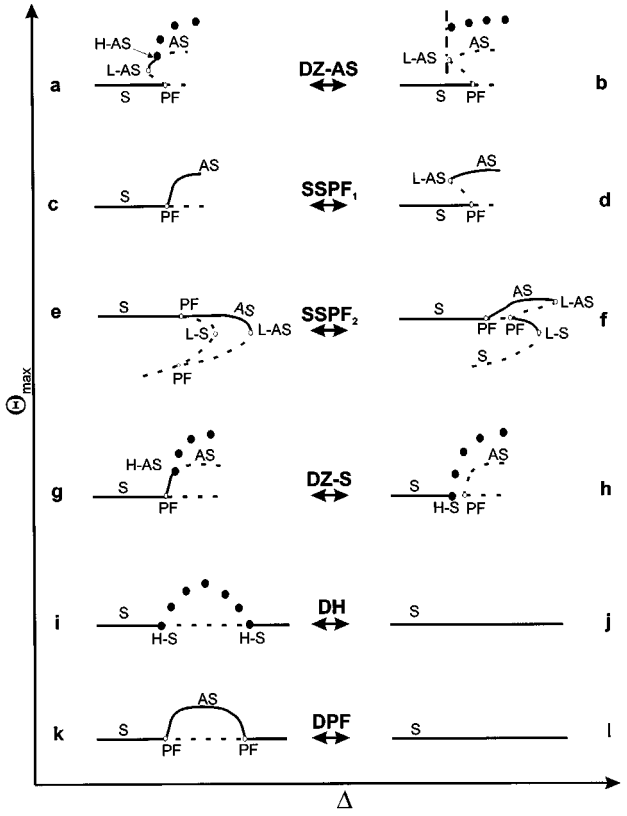

Figure A1. Unfolding of various codimension-2 singular points.

S (AS) = symmetric (asymmetric) states; PF = pitchfork bifurcation; H-S (-AS) = Hopf bifurcation on symmetric (asymmetric) branch; L-S (-AS) = limit point of symmetric (asymmetric) states; solid line = stable; dashed line = unstable.

A *double-zero point on the asymmetric branch* (DZ-AS) is a Hopf bifurcation that exists at the limit point of the branch of asymmetric steady states; that is, at the intersection of the L-AS and the H-AS. Figure A1a and A1b describe the unfoldings of a *DZ-AS*.

A sub-supercritical pitchfork bifurcation (SSPF) is the intersection of the loci of the PF with that of either the (L-S) or (L-AS). A transition of the branch of asymmetric states from subcritical to supercritical occurs at a $SSPF_1$. Thus, next to that point between points L-AS and PF in Figure A1d, stable symmetric and asymmetric steady states exist. At $SSPF_2$, a PF crosses the limit point of the symmetric states (L-S). This also causes a sub- to supercritical transition of the asymmetric branch close to the L-S point (transition of Figure A1e to A1f).

A pitchfork (PF) and a Hopf (H-AS) bifurcation coexist at a *double-zero point on the symmetric branch* (DZ-S). The unfolding of this bifurcation is shown in Figures A1g and A1h. While the asymmetric steady state is stable between PF and H-AS in Figure A1g, following the transition of the Hopf bifurcation at the DZ-S bifurcation, periodic states exist between PF and H-S (Figure A1h).

A limit point of the H-S locus is a *degenerate Hopf bifurcation* (DH). At this singularity, two Hopf-points coalesce and disappear. Consequently, periodic solutions exist on only one side of the DH (Figure $A1_i$ and $A1_j$). Similarly, two pitchfork points coalesce and vanish at a *degenerate pitchfork* (DPF) bifurcation. Therefore, at the DPF singularity, asymmetric steady-state branches appear or vanish (Figures A1k and A1l).

Manuscript received Dec. 17, 1999, and revision received May 10, 2000.